

An exponential integrator for advection-dominated reactive transport in heterogeneous porous media

A. Tambue^{*,a}, G. J. Lord^b, S. Geiger^c

^a*Department of Mathematics and the Maxwell Institute for Mathematical Sciences,
Heriot Watt University, Edinburgh EH14 4AS, U.K.*

^b*Department of Mathematics and the Maxwell Institute for Mathematical Sciences,
Heriot Watt University, Edinburgh EH14 4AS, U.K.*

^c*Institute of Petroleum Engineering and the Edinburgh Collaborative of Subsurface
Science and Engineering, Heriot Watt University, Edinburgh EH14 4AS, U.K.*

Abstract

We present an exponential time integrator in conjunction with a finite volume discretisation in space for simulating transport by advection and diffusion including chemical reactions in highly heterogeneous porous media representative of geological reservoirs. These numerical integrators are based on the variation of constants solution and solving the linear system exactly. This is at the expense of computing the exponential of the stiff matrix comprising the finite volume discretisation. Using real Léja points or a Krylov subspace technique to approximate the exponential makes these methods competitive compared to standard finite difference-based time integrators. We observe for a variety of example applications that numerical solutions with exponential methods are generally more accurate and require less computational cost. They hence comprise an efficient and accurate method for simulating

*Corresponding author

Email addresses: `at150@hw.ac.uk` (A. Tambue), `gabriel@ma.hw.ac.uk` (G. J. Lord), `sebastian.geiger@pet.hw.ac.uk` (S. Geiger)

non-linear advection dominated transport in geological formations.

Key words: Exponential integration, Léja points, Krylov subspace, advection-diffusion equation, fast time integrators, porous media

1. Introduction

Advection and diffusion can transport chemically reactive components such as dissolved minerals, colloids, or contaminants, over long distances through the highly heterogeneous porous media comprising geological formations. It is hence a fundamental process in many geo-engineering applications, including oil and gas recovery from hydrocarbon reservoirs, groundwater contamination and sustainable use of groundwater resources, storing greenhouse gases (e.g, CO₂) or radioactive waste in the subsurface, or mining heat from geothermal reservoirs. One of the fundamental challenges is to forecast these processes accurately because the permeability in heterogeneous porous and fractured media typically varies over orders of magnitude in space and possibly time (e.g, [1, 2]). This causes highly variable flow fields where local transport can be dominated entirely by either advection (Péclet number larger than one) or diffusion (Péclet number less than one), leading to macroscopic mixing and “anomalous transport” that is characterised by early breakthrough of solutes or contaminants and long tailing at late time [3]. Chemical reaction rates and equilibrium constants can vary in a similar manner, giving rise to complex mixing-induced reaction patterns at the macro-scale because chemical reactions rates can dominate locally over transport rates or vice versa (e.g, [4, 5, 6]).

Predicting the spatial spreading and mixing of reactive solutes in field

22 applications hence requires the efficient and accurate numerical solution of
23 advection-diffusion-reaction equations (ADR) which resolve the wide range
24 in flow velocities and reaction rates. This is particularly important because
25 the exact spatial distribution of the permeability field and reaction rates is
26 commonly unknown and therefore a large number of simulations must be
27 run to quantify the uncertainty of the transport behaviour [7], for example
28 to forecast the possible arrival of highly toxic contaminants at a groundwater
29 well and design adequate remediation schemes.

30 The ADR can be discretised in space by the full range of spatial dis-
31 cretisations (e.g, finite differences, finite volumes, or finite elements) and
32 each method comprises its own body of literature. However a fundamental
33 challenge remains. How to integrate in time the system of stiff ODEs, repre-
34 senting transport and reaction processes evolving over multiple time scales,
35 in a stable, accurate and efficient way while avoiding non-physical oscilla-
36 tions (e.g, [8, 9]). The key problem in porous media flow is to overcome the
37 limitations of stability criteria, such as the Courant-Friedrich-Levy criterion,
38 when resolving the huge variation in competing transport and reaction rates.
39 Common methods include implicit or adaptive time-stepping (e.g, [12, 13])
40 and operator splitting techniques (e.g, [10, 11]). Comparatively new meth-
41 ods are streamline-based simulations where transport is computed along the
42 time-of-flight [14, 15], adaptive mesh refinement to focus the computational
43 effort around the moving fronts and resolve them accurately [16], or event-
44 based simulations where only those regions are updated where an event (i.e.
45 chemical reaction or transport) occurs [17, 18].

46 The family of exponential integrators date back to the 1960's (see [19])

47 and [20] for history and detailed references). These methods are based on
48 approximating the corresponding integral formulation of the non-linear part
49 of the differential equation and solving the linear part exactly and com-
50 puting the exponential of a matrix. Sidje [24] used the Krylov subspace
51 technique and Padé approximation to solve the linear system of ODEs based
52 on variation of constants. Cox and Matthews [32] developed the family
53 of exponential time differencing methods for solving non-linear stiff ODEs.
54 They present the instability issue for computing non-diagonal matrix ex-
55 ponential functions, the so called φ -functions. Kassam and Trefethen [20]
56 used a fourth order exponential time differencing method and the contour
57 integral technique for computing the matrix exponential functions to solve
58 the Kuramoto-Sivashinsky and Allen-Cahn PDEs in one dimension. Berland
59 et al. [33] used a Padé approximation to compute the matrix exponential
60 of φ -functions and provided a package for exponential integrators which is
61 efficient in one dimension.

62 Although exponential integrators have the advantage that they solve the
63 linear part exactly in time, this is at the price of computing the exponential
64 of a matrix, a notorious problem in numerical analysis [36]. However, new
65 developments in real fast Léja points and Krylov subspace techniques for
66 computing functions of the matrix exponential has revived interest in these
67 methods. The real fast Léja points technique is based on matrix interpola-
68 tion polynomials at spectral Léja sequences [21, 22]. The Krylov subspace
69 technique is based on the idea of projecting the operator on a “small” Krylov
70 subspace of the matrix via the Arnoldi process [23, 24].

71 In two and three dimensions, the real fast Léja points technique [25, 26,

72 22, 27] and Krylov subspace technique [25, 26] have been used to implement
73 the matrix exponential of φ -functions efficiently in linear advection diffusion
74 equations. The real fast Léja points technique is also used for the exponential
75 Euler-Midpoint integrator scheme for solving non-linear ADRs [28] and for
76 the exponential Rosenbrock-type integrators for solving semi-linear parabolic
77 PDEs [29]. Simulations have been carried out for homogeneous media with
78 constant dispersion tensors, uniform velocity fields, and low Péclet number
79 flows using finite difference methods or finite element methods for spatial dis-
80 cretisations. In contrast to previous work, we consider heterogeneous media,
81 the exponential time differencing method of order one with the finite volume
82 discretisation in space and examine high Péclet number flows.

83 The aim of this paper is to investigate the exponential time differencing
84 method of order one (ETD1) and compare its performance in terms of ef-
85 ficiency and accuracy to standard semi-implicit and fully implicit schemes
86 for solution of non-linear ADRs in highly heterogeneous porous media with
87 largely varying Péclet number flows, that is situations where transport is
88 locally dominated either by diffusion or advection. We use 2D simulations
89 and finite volume discretisations to demonstrate the efficiency and the accu-
90 racy of the exponential scheme ETD1. In the implementation of the ETD1
91 scheme we also compare the efficiency of the real fast Léja points technique
92 with the Krylov technique for computing matrix exponential.

93 The paper is organised as follows. In the next section we present the
94 mathematical and numerical formulations of ADR. Then we discuss the ex-
95 ponential time differencing stepping schemes for ADR and implementation
96 of the exponential time differencing of order one (ETD1) using the real fast

97 Léja points and Krylov space techniques. This is followed by two sets of tests
 98 in 2D from homogeneous porous media with exact solutions. This allows us
 99 to examine the ETD1 scheme as well as test feasibility for large systems. We
 100 then consider heterogeneous porous media where we take first a deterministic
 101 permeability field and then a random permeability field. In these examples
 102 we see that the ETD1 method using the real Léja points technique is efficient
 103 and competitive compared to standard finite difference time integrators. Fi-
 104 nally, the discussions and conclusions are given.

105 **2. Mathematical and numerical formulations**

106 *2.1. Model problem*

107 Our model problem is to find the unknown concentration of the solute C
 108 that satisfies the following advection-diffusion-reaction equation (ADR):

$$\phi(\underline{x}) \frac{\partial C}{\partial t} = \nabla \cdot (\mathbf{D}(\underline{x}) \nabla C) - \nabla \cdot (\mathbf{q}(\underline{x}) C) + R(\underline{x}, C) \quad (\underline{x}, t) \in \Omega \times [0, T]. \quad (1)$$

109 Here we take Ω to be an open domain of \mathbb{R}^2 and solve over a finite time
 110 interval $[0, T]$. ϕ is the porosity (void fraction) of the rock, and \mathbf{D} is the
 111 symmetric dispersion tensor. For simplicity we take \mathbf{D} to be

$$\mathbf{D} = \begin{pmatrix} D_1 & 0 \\ 0 & D_2 \end{pmatrix} \quad (2)$$

112 with $D_1 > 0, D_2 > 0$. The term R is a reaction function. Possible reaction
 113 mechanisms can be adsorption, for example as described by a Langmuir
 114 isotherm, biodegradation or radioactive decay. The velocity \mathbf{q} is given by
 115 Darcy's law as

$$\mathbf{q} = -\frac{k(\underline{x})}{\mu} \nabla p, \quad (3)$$

where p is the fluid pressure, μ is the fluid viscosity, and k the permeability of the porous medium. Assuming that rock and fluids are incompressible and sources or sinks are absent, mass conservation is given by $\nabla \cdot \mathbf{q} = 0$. From this we can formulate the elliptic pressure equation, which allows us to compute the pressure field in the porous medium

$$\nabla \cdot \left[\frac{k(\underline{x})}{\mu} \nabla p \right] = 0. \quad (4)$$

116 2.2. Space discretisation

117 We use the classical finite volume method with a structured mesh \mathcal{T} [30].
 118 First, we solve the pressure equation (Eq. (4)) and then obtain the velocity
 119 field from Eq. (3). This provides the integral of the velocity $\{q_{i,j}\}_{i \in \mathcal{T}}$ at each
 120 edge j of a control volume i . Integrating Eq. (1) over i , using the divergence
 121 theorem and the flux approximations used in [30] we obtain the following
 122 equation

$$\phi_i V_i \frac{dC_i(t)}{dt} = - \sum_j^{\text{edges of } i} [F_{i,j}(t) + q_{i,j} C_j(t)] + V_i R(C_i(t)) \quad \forall i \in \mathcal{T}. \quad (5)$$

123 Here, $C_i(t)$ is the approximation of C at time t at the center of the control
 124 volume $i \in \mathcal{T}$, $F_{i,j}(t)$ is the approximation of the diffusive flux at time t at
 125 edge j and $q_{i,j} C_j(t)$ is the approximation of the advective flux at time t at
 126 edge j . $V_i R(C_i(t))$ is the approximation of the integral of the reaction term
 127 over the i th control volume of area V_i and ϕ_i is the mean value of the porosity
 128 ϕ in the control volume i . We apply standard upwind weighting [31, 30] to
 129 the flux term $q_{i,j} C_j$.

130 We let h denote the maximum mesh size and use this to indicate our
 131 spatial discretisation. We can rewrite Eq. (5) in the standard way [31] as the

132 following non-linear system of equations for all control volumes $i \in \mathcal{T}$

$$\frac{d\underline{\mathbf{C}}_h(t)}{dt} = \mathbf{L}\underline{\mathbf{C}}_h(t) + \underline{\mathbf{N}}(\underline{\mathbf{C}}_h, t), \quad t \in [0, T]. \quad (6)$$

133 Here \mathbf{L} is the stiffness matrix coming from the approximations of the ad-
 134 vective and diffusive fluxes, $\underline{\mathbf{C}}_h(t)$ is the concentration vector at all control
 135 volumes at time t , and the term $\underline{\mathbf{N}}(\underline{\mathbf{C}}_h, t)$ comes from the boundary condi-
 136 tions and reaction term. In section 4, we also examine the effects of putting
 137 the approximation of the advective flux in the non-linear term $\underline{\mathbf{N}}(\underline{\mathbf{C}}_h, t)$.

138 2.3. Standard time discretisation

139 We briefly describe two standard time-stepping schemes, the implicit Eu-
 140 ler scheme and the semi implicit Euler scheme. Later we use these for com-
 141 parison with the exponential scheme of order one, ETD1. Given the initial
 142 data $\underline{\mathbf{C}}_h^0 = \underline{\mathbf{C}}^0$, the implicit Euler scheme for Eq. (6) is

$$\frac{\underline{\mathbf{C}}_h^{n+1} - \underline{\mathbf{C}}_h^n}{\Delta t} = \mathbf{L}\underline{\mathbf{C}}_h^{n+1} + \underline{\mathbf{N}}(\underline{\mathbf{C}}_h^{n+1}, t_{n+1}) \quad (7)$$

143 and the semi implicit scheme is

$$\frac{\underline{\mathbf{C}}_h^{n+1} - \underline{\mathbf{C}}_h^n}{\Delta t} = \mathbf{L}\underline{\mathbf{C}}_h^{n+1} + \underline{\mathbf{N}}(\underline{\mathbf{C}}_h^n, t_n) \quad (8)$$

144 where $\Delta t = t_{n+1} - t_n$ is the fixed time-step. For the implicit Euler method
 145 we have to solve a non-linear algebraic equation of the form

$$\underline{\mathbf{f}}(\underline{\mathbf{X}}) = (\mathbf{I} + \Delta t \mathbf{L})\underline{\mathbf{X}} + \Delta t \underline{\mathbf{N}}(\underline{\mathbf{X}}, t_n) - \underline{\mathbf{C}}_h^n = \underline{\mathbf{0}}$$

146 at each time-step. For brevity we denote $\underline{\mathbf{C}}_h^{n+1}$ as $\underline{\mathbf{X}}$. We use Newton's method
 147 and a variant of Newton's method designed for semi-linear problems [31].
 148 We solve the linear systems using the standard solver in MatlabTM at each

149 iteration in the exact Newton's method. For the variant of Newton's method,
 150 the Jacobian of \underline{f} , $\mathbf{J}(\underline{X})$, is approximated by its constant linear part so that
 151 $\mathbf{J}(\underline{X}) \approx \mathbf{I} + \Delta t \mathbf{L}$. The corresponding quasi Newton's iteration is then given
 152 by

$$\begin{aligned} \underline{X}_{k+1} &= \underline{X}_k - (\mathbf{I} + \Delta t \mathbf{L})^{-1} \underline{f}(\underline{X}_k) \\ &= (\mathbf{I} + \Delta t \mathbf{L})^{-1} (\Delta t \underline{N}(\underline{X}_k, t_n) - \underline{C}_h^n). \end{aligned}$$

153 This is equivalent to a fixed point method to solve the equivalent equation
 154 $(\mathbf{I} + \Delta t \mathbf{L})^{-1} \underline{f}(\underline{X}) = \underline{0}$. The approximation of the Jacobian by its constant
 155 linear part allows us to compute the matrix factorisation only once and to
 156 reuse this at each time-step. In the quasi-exact Newton's method and the
 157 semi implicit Euler scheme we solve the linear systems using either an LU-
 158 decomposition or the standard solver in MatlabTM.

159 3. Exponential Time Differencing scheme of order one for ADR

160 3.1. Review of the Exponential Time Differencing methods

161 We introduce the exponential time differencing stepping scheme of order
 162 one (ETD1) for the ADR problem (Eq. (1)) using the variation of constants.
 163 This allows us to write the exact solution of Eq. (6) as

$$\underline{C}_h(t_n) = e^{t_n \mathbf{L}} \underline{C}^0 + e^{t_n \mathbf{L}} \int_0^{t_n} e^{-s \mathbf{L}} \underline{N}(\underline{C}_h(s), s) ds, \quad t_n = n \Delta t \in [0, T]$$

164 where s is the integration time. Then, given the exact solution at the time
 165 t_n , we can construct the corresponding solution at t_{n+1} as

$$\underline{C}_h(t_{n+1}) = e^{\Delta t \mathbf{L}} \underline{C}_h(t_n) + e^{\Delta t \mathbf{L}} \int_0^{\Delta t} e^{-s \mathbf{L}} \underline{N}(\underline{C}_h(t_n + s), t_n + s) ds. \quad (9)$$

Note that the expression in Eq. (9) is still an exact solution. The idea behind exponential time differencing is to approximate $\underline{\mathbf{N}}(\underline{\mathbf{C}}_h(t_n + s), t_n + s)$ by a suitable polynomial [32, 20]. We consider the simplest case where $\underline{\mathbf{N}}(\underline{\mathbf{C}}_h(t_n + s), t_n + s)$ is approximated by the constant $\underline{\mathbf{N}}(\underline{\mathbf{C}}_h(t_n), t_n)$ and for simplicity consider a constant time-step $\Delta t = t_{n+1} - t_n$. The corresponding ETD1 scheme is given by

$$\underline{\mathbf{C}}_h^{n+1} = e^{\Delta t \mathbf{L}} \underline{\mathbf{C}}_h^n + \Delta t \varphi_1(\Delta t \mathbf{L}) \underline{\mathbf{N}}(\underline{\mathbf{C}}_h^n, t_n) \quad (10)$$

166 where $\varphi_1(\mathbf{G}) = \mathbf{G}^{-1} (e^{\mathbf{G}} - \mathbf{I}) = (e^{\mathbf{G}} - \mathbf{I}) \mathbf{G}^{-1}$ for any invertible matrix \mathbf{G} .

167 Note that the ETD1 scheme in Eq. (10) can be rewritten as

$$\underline{\mathbf{C}}_h^{n+1} = \underline{\mathbf{C}}_h^n + \Delta t \varphi_1(\Delta t \mathbf{L}) (\mathbf{L} \underline{\mathbf{C}}_h^n + \underline{\mathbf{N}}(\underline{\mathbf{C}}_h^n, t_n)). \quad (11)$$

168 This new expression has the advantage that it is computationally more effi-
 169 cient as only one matrix exponential function needs to be evaluated at each
 170 step.

171 3.2. Efficient computation of the action of φ_1

172 It is well known that a standard Padé approximation for a matrix expo-
 173 nential is not an efficient method for large scale problems [24, 33, 36]. Here
 174 we focus on the real fast Léja points and the Krylov subspace techniques to
 175 evaluate the action of the exponential matrix function $\varphi_1(\Delta t \mathbf{L})$ on a vector
 176 $\underline{\mathbf{v}}$, instead of computing the full exponential function $\varphi_1(\Delta t \mathbf{L})$ as in a stan-
 177 dard Padé approximation. The details of the real fast Léja points technique
 178 and [23, 24] for the Krylov subspace technique are given in [27, 21, 22]. We
 179 give a brief summary below.

180 *3.2.1. Real fast Léja points technique*

181 For a given vector \underline{v} , real fast Léja points approximate $\varphi_1(\Delta t \mathbf{L})\underline{v}$ by
 182 $P_m(\Delta t \mathbf{L})\underline{v}$, where P_m is an interpolation polynomial of degree m of φ_1 at the
 183 sequence of points $\{\xi_i\}_{i=0}^m$ called spectral real fast Léja points. These points
 184 $\{\xi_i\}_{i=0}^m$ belong to the spectral focal interval $[\alpha, \beta]$ of the matrix $\Delta t \mathbf{L}$, i.e. the
 185 focal interval of the smaller ellipse containing all the eigenvalues of $\Delta t \mathbf{L}$.
 186 This spectral interval can be estimated by the well known Gershgorin circle
 187 theorem [34]. It has been shown that as the degree of the polynomial increases
 188 and hence the number of Léja points increases, convergence is achieved [27],
 189 i.e.

$$\lim_{m \rightarrow \infty} \|\varphi_1(\Delta t \mathbf{L})\underline{v} - P_m(\Delta t \mathbf{L})\underline{v}\|_2 = 0, \quad (12)$$

190 where $\|\cdot\|_2$ is the standard Euclidian norm. For a real interval $[\alpha, \beta]$, a
 191 sequence of real fast Léja points $\{\xi_i\}_{i=0}^m$ is defined recursively as follows.
 192 Given an initial point ξ_0 , usually $\xi_0 = \beta$, the sequence of fast Léja points is
 193 generated by

$$\prod_{k=0}^{j-1} |\xi_j - \xi_k| = \max_{\xi \in [\alpha, \beta]} \prod_{k=0}^{j-1} |\xi - \xi_k| \quad j = 1, 2, 3, \dots \quad (13)$$

194 We use the Newton's form of the interpolating polynomial P_m given by

$$P_m(z) = \varphi_1[\xi_0] + \sum_{j=1}^m \varphi_1[\xi_0, \xi_1, \dots, \xi_j] \prod_{k=0}^{j-1} (z - \xi_k) \quad (14)$$

195 where the divided differences $\varphi_1[\bullet]$ are defined recursively by

$$\begin{cases} \varphi_1[\xi_j] = \varphi_1(\xi_j) \\ \varphi_1[\xi_j, \xi_{j+1}, \dots, \xi_k] := \frac{\varphi_1[\xi_{j+1}, \xi_{j+2}, \dots, \xi_k] - \varphi_1[\xi_j, \xi_{j+1}, \dots, \xi_{k-1}]}{\xi_k - \xi_j} \end{cases} \quad (15)$$

Algorithm 1 : Compute $\varphi_1(\Delta t \mathbf{L})\underline{v}$ with real fast Léja points. Error e_m is controlled to a prescribed tolerance tol so that $e_m^{\text{Léja}} < tol$.

- 1: **Input:** $\mathbf{L}, \underline{v}, \Delta t, tol, z$ {matrix, vector, time-step, tolerance, number of Léja points to be generated }
 - 2: $[\alpha, \beta] = \text{getfocal}(\mathbf{L})$ {get the focal interval using the Gershgorin circle theorem [34]}
 - 3: $\xi = \text{getLeja}(\alpha, \beta, z)$ {generate z fast Léja points from (Eq. (13)).}
 - 4: $d_0 = \varphi_1(\xi_0)$.
 - 5: $\underline{w}_0 = \underline{v}, \underline{p}_0 = d_0 \underline{w}_0, m = 0$ {initialisation}
 - 6: **while** $e_m^{\text{Léja}} = |d_m| \times \|\underline{w}_m\|_2 > tol$ **do**
 - 7: $\underline{w}_{m+1} = (\Delta t \mathbf{L} - \xi_m \mathbf{I}) \underline{w}_m$
 - 8: $m = m + 1$
 - 9: $d_m = \varphi_1(\xi_m)$
 - 10: **for** $i = 1, \dots, m$ **do**
 - 11: $d_m = \frac{d_m - d_{i-1}}{\xi_m - \xi_{i-1}}$ {compute the next divided difference d_m }
 - 12: **end for**
 - 13: $\underline{p}_m = \underline{p}_{m-1} + d_m \underline{w}_m$
 - 14: **end while**
 - 15: **Output:** \underline{p}_m
-

196 We summarise in Algorithm 1 the steps for computing $\varphi_1(\Delta t \mathbf{L})\underline{\mathbf{v}}$. In our
 197 implementation we estimate the focal interval for \mathbf{L} only once and precom-
 198 pute a sufficiently large number z of Léja points using the efficient algorithm
 199 of Baglama et al. [21] for a focal interval of $\Delta t \mathbf{L}$.

200 The data is passed as input parameters during each call of the algorithm
 201 and scaled by Δt . We observed the same convergence problems as described
 202 by Caliori et al. [27], that is problems arising from round-off errors during
 203 the computation of the divided differences (Eq. (15)) and from the large
 204 capacity of the spectral focal interval $[\alpha, \beta]$. We were able to resolve this
 205 issue by reducing the time-step size or by using an algorithm for minimising
 206 rounding errors from the divided differences [35] when computing Eq. (15).
 207 Note that although it is advised in [27] to compute the divided differences in
 208 quadruple precision we did not find this necessary.

209 3.2.2. Krylov space subspace technique

210 The main idea of the Krylov subspace technique is to approximate the
 211 action of the exponential matrix function $\varphi_1(\Delta t \mathbf{L})$ on a vector $\underline{\mathbf{v}}$ by projec-
 212 tion onto a small Krylov subspace $K_m = \text{span}\{\underline{\mathbf{v}}, \mathbf{L}\underline{\mathbf{v}}, \dots, \mathbf{L}^{m-1}\underline{\mathbf{v}}\}$ [24]. The
 213 approximation is formed using an orthonormal basis of $\mathbf{V}_m = [\underline{\mathbf{v}}_1, \underline{\mathbf{v}}_2, \dots, \underline{\mathbf{v}}_m]$
 214 of the Krylov subspace K_m and of its completion $\mathbf{V}_{m+1} = [\mathbf{V}_m, \underline{\mathbf{v}}_{m+1}]$. The
 215 basis is found by Arnoldi iteration [37] which uses stabilised Gram-Schmidt
 216 to produce a sequence of vectors that span the Krylov subspace (see Algo-
 217 rithm 2).

218 Let $\underline{\mathbf{e}}_i^j$ be the i^{th} standard basis vector of \mathbb{R}^j . We approximate $\varphi_1(\Delta t \mathbf{L})\underline{\mathbf{v}}$

219 by

$$\varphi_1(\Delta t \mathbf{L})\underline{\mathbf{y}} \approx \|\underline{\mathbf{y}}\|_2 \mathbf{V}_{m+1} \varphi_1(\Delta t \overline{\mathbf{H}}_{m+1}) \underline{\mathbf{e}}_1^{m+1} \quad (16)$$

with

$$\overline{\mathbf{H}}_{m+1} = \begin{pmatrix} \mathbf{H}_m & \underline{\mathbf{0}} \\ 0, \dots, 0, h_{m+1,m} & 0 \end{pmatrix} \quad \text{where} \quad \mathbf{H}_m = \mathbf{V}_m^T \mathbf{L} \mathbf{V}_m = [h_{i,j}].$$

220 The coefficient $h_{m+1,m}$ is recovered in the last iteration of Arnoldi's iteration.

221 For a small Krylov subspace (i.e, m is small) a standard Padé approxi-
 222 mation can be used to form $\varphi_1(\Delta t \overline{\mathbf{H}}_{m+1})$, but a efficient way used in [24]
 223 is to recover $\varphi_1(\Delta t \overline{\mathbf{H}}_{m+1}) \underline{\mathbf{e}}_1^{m+1}$ directly from the Padé approximation of the
 224 exponential of a matrix related to \mathbf{H}_m [24]. In our implementation we use
 225 the function `phiv.m` of the package Expokit [24], which allows us to compute
 226 the forward ETD1 solution using the previous solution while controlling the
 227 local error at each iteration for a given tolerance. The function `phiv.m` takes
 228 the time step Δt , the matrix \mathbf{L} , the vectors $\underline{\mathbf{u}}$ and $\underline{\mathbf{v}}$, the dimension of the
 229 Krylov subspace m , and the desired tolerance as the input and provides
 230 $\underline{\mathbf{u}} + \Delta t \varphi_1(\Delta t \mathbf{L})(\mathbf{L}\underline{\mathbf{u}} + \underline{\mathbf{v}})$ as the output. This method is accurate for a sym-
 231 metric matrix with negative eigenvalues but can be less efficient on very large
 232 non-symmetric matrices [23, 24].

233 4. Numerical experiments

234 To analyse the convergence and efficiency of the ETD1 method for solving
 235 ADRs, we apply it to a variety of porous media flow problems and compare
 236 it to our standard time-stepping methods implicit Euler and semi implicit
 237 schemes introduced in Section 2.3. We consider the following four problems:

Algorithm 2 : Arnoldi's algorithm

```
1: Initialise:  $\underline{v}_1 = \frac{\underline{v}}{\|\underline{v}\|_2}$  {normalisation}
2: for  $j = 1 \cdots m$  do
3:    $\underline{w} = \mathbf{L}\underline{v}_j$ 
4:   for  $i = 1 \cdots j$  do
5:      $h_{i,j} = \underline{w}^T \underline{v}_i$  {compute inner product to build elements of the matrix
       $\mathbf{H}$ }
6:      $\underline{w} = \underline{w} - h_{i,j}\underline{v}_i$  {Gram-Schmidt process}
7:   end for
8:    $h_{j+1,j} = \|\underline{w}\|_2$ 
9:    $\underline{v}_{j+1} = \frac{\underline{w}}{\|\underline{w}\|_2}$  {normalisation}
10: end for
```

- 238 1. A linear ADR without reaction term, a heterogeneous dispersion tensor,
239 and a non-uniform velocity field representing moderate Péclet number
240 flows, for which an analytical solution exists [38].
- 241 2. A non-linear ADR in homogeneous media where transport is controlled
242 equally by advection and diffusion (i.e, Péclet number is 1) for which
243 an analytical solution exists [28].
- 244 3. A non-linear ADR for a deterministic permeability field representing
245 a highly idealised fractured porous media. Here transport is entirely
246 dominated by advection (high Péclet number flow).
- 247 4. A non-linear ADR for a stochastically generated permeability field
248 where transport is locally dominated by either advection or diffusion.

In the two latter applications we use the classical Langmuir isotherm to model the sorption of the transported species onto the rock surface, i.e.

$$R(C) = \frac{\lambda\beta C}{1 + \lambda C}.$$

249 The parameter λ is an adsorption constant and β the maximum amount of
 250 the solute that can be adsorbed. We take $\lambda = \beta = 1$ in this work.

251 For the sake of simplicity we assume that the porosity ϕ is constant in
 252 all applications. In all cases we take our domain to be rectangular $\Omega =$
 253 $[0, L_1) \times [0, L_2)$ but use both, uniform and non-uniform, rectangular meshes.
 254 The time has been normalised by the average flow rate and the domain length
 255 in the direction of flow such that the mean of the concentration has traveled
 256 through the entire domain at $T = 1$. In each application example, the matrix
 257 \mathbf{L} is pentadiagonal. For a grid size $N_x \times N_y$, the corresponding matrix has
 258 the size $N_x N_y \times N_x N_y$ with $5 \times N_x N_y - 2 \times N_x - 6$ non-zero elements.

259 For pressure, we take the Dirichlet boundary $\Gamma_D^1 = \{0, L_1\} \times [0, L_2]$ and
 260 Neumann boundary $\Gamma_N^1 = (0, L_1) \times \{0, L_2\}$ such that

$$p = \begin{cases} 1 & \text{in } \{0\} \times [0, L_2] \\ 0 & \text{in } \{L_1\} \times [0, L_2] \end{cases}$$

$$-k \nabla p(x, t) \cdot \underline{\mathbf{n}} = 0 \quad \text{in } \Gamma_N^1.$$

261 For concentration, we take the Dirichlet boundary $\Gamma_D = \{0\} \times [0, L_2]$ and
 262 Neumann boundary $\Gamma_N = \{(0, L_1] \times \{0, L_2\}\} \cup \{\{L_1\} \times [0, L_2]\}$ such that

$$\begin{aligned} C &= 1 && \text{in } \Gamma_D \times [0, T] \\ -(\mathbf{D}\nabla C)(x, t) \cdot \underline{\mathbf{n}} &= 0 && \text{in } \Gamma_N \times [0, T] \\ C_0 &= 0 && \text{in } \Omega \quad (\text{initial solution}) \end{aligned}$$

263 where $\underline{\mathbf{n}}$ is the unit outward normal vector to Γ_N (or Γ_N^1).

264 We report below the local or grid Péclet number $\text{Pe}_{\text{loc}} = \max_i \text{Pe}_i$ where
 265 Pe_i is computed over each control volume as

$$\text{Pe}_i := \frac{\max_{j \text{ edge of } i} |q_{i,j}|}{\|\mathbf{D}_i\|_\infty}.$$

266 \mathbf{D}_i is the mean value of the diffusion matrix over the control volume i and
 267 $q_{i,j}$ is the integral of the velocity over the edge j for the control volume i .

268 For applications where we do not have an analytic solution we estimate
 269 the global error by

$$\|C_h(t) - C_h^{\Delta t}(t)\|_{L^2(\Omega)} \approx 2\|C_h^{\Delta t}(t) - C_h^{\Delta t/2}(t)\|_{L^2(\Omega)}.$$

270 where $C_h^{\Delta t}(t)$ is the approximation of the solution at time t found with time-
 271 step Δt . Unless explicitly stated, the tolerance used for Newton's method
 272 and the ETD1 schemes is 10^{-6} and the Krylov space dimension used is $m = 6$.
 273 The tests were performed on a standard PC with a 3 GHz processor and 2GB
 274 RAM. Our code was implemented in Matlab 7.7. In the legends of all of our
 275 graphs we use the following notation

- 276 • “Implicit with Newton” denotes results from the implicit Euler with
 277 standard Newton method.

- 278 • “Implicit with Newton V” denotes results from the implicit Euler with
279 the variant of Newton method.
- 280 • “Léja ETD1” denotes results from ETD1 with real fast Léja points for
281 matrix exponential.
- 282 • “Krylov ETD1” denotes results from ETD1 with Krylov subspace for
283 matrix exponential.
- 284 • “Semi implicit” denotes results from the semi-implicit scheme.

285 *4.1. Homogeneous porous media without reaction term*

286 We use this problem to examine the scaling of the ETD1 method for
287 problems with different numbers of unknowns and analyse the convergence
288 in space by comparing it to an exact solution [38]. Since the ADR does
289 not contain a reaction term, the problem is linear. The domain is defined
290 as $\Omega = [L_0, L_1) \times [L_0, L_1)$, $L_0 = 0.01$, $L_1 = 2$. The initial time is given
291 as $t_0 = 0.01$. This is necessary because the exact solution is not defined at
292 the origin and at $t = 0$. The dispersion tensor \mathbf{D} is heterogeneous and its
293 coefficients are given by

$$\begin{cases} D_1(x, y) = D_0 u_0^2 x^2 & (x, y) \in \Omega \\ D_1(x, y) = D_0 u_0^2 y^2 & (x, y) \in \Omega. \end{cases}$$

294 The velocity field (Fig. 1(a)) is given explicitly by

$$\begin{cases} \mathfrak{q} = (q_x, q_y)^T \\ q_x(x, y) = u_0 x & (x, y) \in \bar{\Omega} \\ q_y(x, y) = -u_0 y & (x, y) \in \bar{\Omega} \end{cases} \quad (17)$$

295 where $D_0 = 0.1$ and $u_0 = 2$. The local Péclet number ranges from 21 to 2 as
 296 the grid is refined. Initial and boundary conditions are taken according to the
 297 exact solution [38], assuming an instantaneous release at a point (x_0, y_0) , $x_0 =$
 298 1.5 , $y_0 = 1.5$. We take a fixed time-step of $\Delta t = 1/3000$.

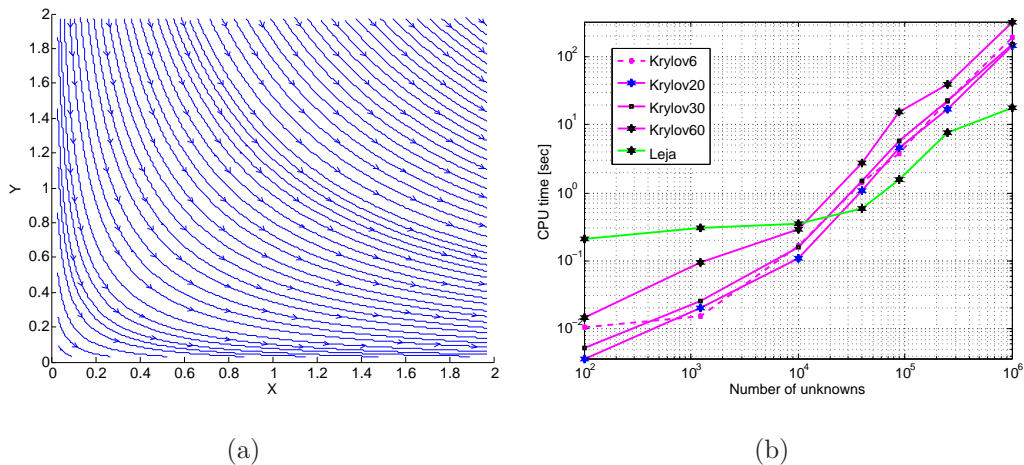


Figure 1: Numerical examples for the linear advection-diffusion problem in homogeneous porous media given in [38] (a) shows the streamlines, (b) shows the CPU time as a function of number of unknowns required to evaluate the expression $\varphi_1(\Delta t \mathbf{L})(\mathbf{L} \mathbf{C}_h^0 + \mathbf{N}(\mathbf{C}_h^0, T_0))$. A standard PC with a 3 GHz processor and 2GB RAM was used for the simulations. The number in the four Krylov curves in (b) denotes the dimension m of the subspace taken.

299 Figure 1(a) shows the streamlines which indicate direction of flow. Fig-
 300 ure 1(b) shows the CPU time needed to compute single time-step using ETD1
 301 with real Léja points and Krylov techniques as a function of the number of
 302 unknowns. The number of the real fast Léja points used to achieve the given
 303 tolerance are 6 for 100 unknowns, and increases to 69 as the grid is refined.

304 In Figure 1(b) we show that good values for the dimension of the Krylov
 305 subspace are $m = 20$ and $m = 6$, but $m = 20$ appears to be a slightly better
 306 value for this specific example. To our knowledge, there is no rigorous theory

307 that allows us to predict the optimal value for m a priori. For example,
 308 the default value used in [24] is $m = 30$ but we observe that this is not
 309 the optimal value for our specific example. When m increases, the total
 310 number of iterations decreases but a penalty occurs due to the additional time
 311 spent in the orthogonalisation process in Algorithm 2 and the corresponding
 312 increase in memory requirements. For small m , a penalty can arise from an
 313 increase in the number of iterations necessary to achieve a given tolerance,
 314 especially if Δt is large, but less time is spent in the orthogonalisation process
 315 and the required memory is lower. Since the memory on the PC used in
 316 this work is limited to 2 GB, the values of Δt in our application examples
 317 are generally small, and we require to compute the action of the matrix
 318 exponential function φ_1 on a vector to reach the final time T over 3000
 319 times, we have chosen $m = 6$ as the optimal value for the Krylov subspace
 320 dimension in all our applications.

321 For 10^4 and more unknowns, that is for problem sizes that become repre-
 322 sentative for real reservoir simulations, the computation of the matrix expo-
 323 nential with real fast Léja points is more efficient than the Krylov technique
 324 by a factor of approximately 10, regardless of the Krylov subspace dimension
 325 m . Similar results were obtained by [25, 26] for constant dispersion tensor,
 326 constant velocity, and low Péclet number flows. Once the matrix size is
 327 greater or equal to 10^4 , the CPU time increases linearly with the number of
 328 unknowns (Figure 1(b)). The time to evaluate a matrix with 10^6 unknowns
 329 using 69 real Léja points is 18 seconds. These results suggest that the ETD1
 330 is a scalable solver and is hence probably applicable to large-scale problems
 331 with several million of unknowns that are encountered in 3D reservoir simu-

332 lations.

333 Figure 2(a) shows a convergence of order $\mathcal{O}(h)$ for the spatial discretisa-
334 tion with fixed time step $\Delta t = 1/3000$. The error in the L^2 norm is computed
335 at time $T = 1$. Figure 2(b) shows the L^2 error as a function CPU time, which
336 is depicted in Figure 2(a).

337 The efficiency for solving this linear ADR problem is roughly similar for
338 all methods, that is approximately the same computational cost is required
339 to reduce the numerical error by a certain increment. Although Figure 1(b)
340 indicates that for small number of unknowns the Krylov technique requires
341 significantly less computational effort than the real Léja point method to
342 compute one step with one vector \underline{v} , Figure 2(b) shows that over the course
343 of an entire simulation, which involves many individual time-steps, the local
344 error control reduces this efficiency, therefore Krylov and Léja point methods
345 are comparable. We recall that the Krylov subspace implementation is known
346 to be efficient for symmetric matrices. Here we observe good convergence
347 even for highly nonsymmetric matrices \mathbf{L} .

348 4.2. Homogeneous porous media with a non-linear reaction term

We now evaluate the ETD1 method for a non-linear ADR problem where
the non-linear reaction term is given by $R(C) = -\gamma C^2(1 - C)$. We take
 $\gamma = 100$, use a constant velocity of $\underline{q} = [-0.01, -0.01]^T$, and the dispersion
tensor has the entries $D_1 = D_2 = 10^{-4}$. The domain is $\Omega = [0, 1) \times [0, 1)$,
which we discretise with $h = \Delta x = \Delta y = 10^{-2}$. The local Péclet number
for the flow is 1, that is transport is controlled equally by advection and
diffusion. The initial condition and boundary conditions are defined with

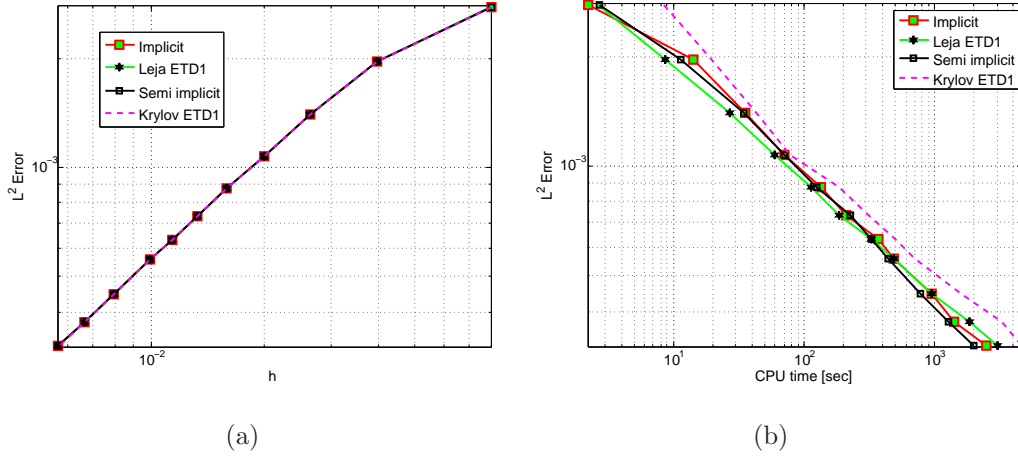


Figure 2: (a) Convergence of the L^2 norm at $T = 1$ as a function of the grid size h . (b) The L^2 norm at $T = 1$ as a function of CPU time. Both plots are for the linear ADR in homogeneous porous media without a reaction term (Problem 1) with fixed $\Delta t = 1/3000$. Recall here that the Krylov subspace dimension is fixed to be $m = 6$.

respect to the exact solution [28] given by

$$C(x, y, t) = (1 + \exp(a(x + y - bt) + a(b - 1)))^{-1} \quad (18)$$

349 where $a = \sqrt{\gamma/(4 \times 10^{-4})}$ and $b = -0.02 + \sqrt{\gamma \times 10^{-4}}$.

350 Figure 3(a) shows the convergence as a function of the chosen time-step
 351 Δt , measuring the error at the final time $T = 1$. The semi-implicit time-
 352 stepping method and the ETD1 methods have similar error constants. All
 353 schemes have the same rate of convergence $\mathcal{O}(\Delta t)$.

354 Figure 3(b) shows the L^2 error as a function of CPU time, which is given
 355 in Figure 3(a). Again, the computational effort to reduce the numerical by a
 356 certain error is approximately equivalent for both, Léja and Krylov subspace
 357 techniques. They are also similar to a semi-implicit time integrator. However,
 358 all three methods, ETD1 with Léja points and Krylov subspace technique and

359 semi-implicit time-stepping, outperform the implicit time-stepping methods.
 360 Those require about 10 times more computational costs to obtain the same
 361 numerical error. If the advective component of the flux is included in the
 362 non-linear part rather than the linear part for the ETD1 scheme, then the
 363 error constant worsens. In this case the graph representing the error would
 364 lie between that of the ETD1 or semi-implicit error and implicit error in
 365 Figure 3(a).

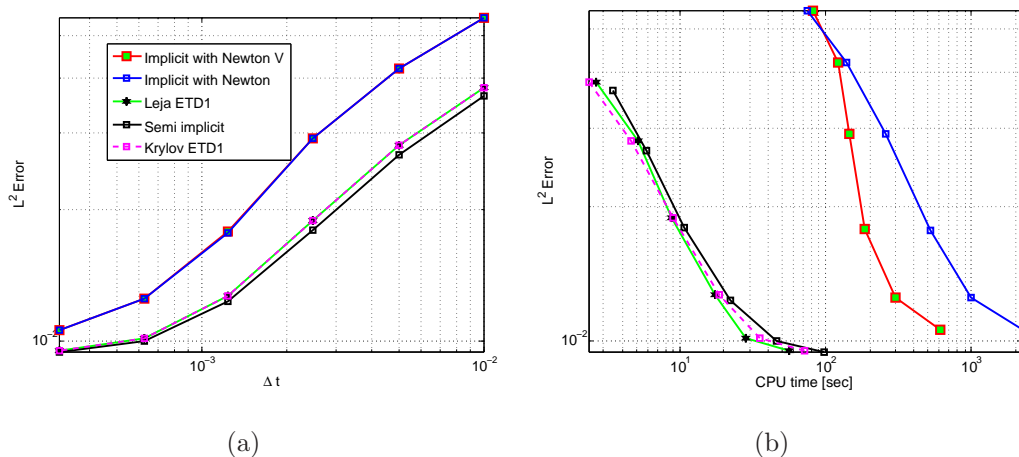


Figure 3: (a) Convergence of the L^2 norm at $T = 1$ as a function of Δt . (b) The L^2 norm at $T = 1$ as a function of CPU time. Both are for the the non-linear ADR in homogeneous porous media (Problem 2).

366 4.3. Deterministic heterogeneous porous media and non-linear reaction

367 We now test the ETD1 method for a porous media with three parallel
 368 high-permeability streaks. This could represent, for example, transport in
 369 a highly idealised fracture pattern. The permeability of the three parallel
 370 streaks is 100 times greater than the permeability of the surrounding domain
 371 (Figure 4(a)). Hence flow is diverted from the lower-permeability rocks into

372 the high-permeability matrix (Figure 4(b)). The advection rates increase to-
373 wards the high-permeability streaks and are highest in them. This is clearly
374 visible by the closer spacing of the streamlines in the high-permeability
375 streaks (Figure 4(b)).

376 For the non-linear reaction term we now take the Langmuir sorption
377 isotherm. The domain is given by $\Omega = [0, 2) \times [0, 3)$ and discretised in
378 space with $\Delta x = 3/50$ and $\Delta y = 1/25$. The dispersion tensor is anisotropic
379 with $D_1 = 10^{-3}$, $D_2 = 10^{-4}$. The viscosity is $\mu = 0.1$. The maximum local
380 Péclet number is 2975.4.

381 Figure 4(c) shows the concentration at $t = 0.3$ and Figure 4(d) the con-
382 centration at $T = 1$. Again, the flow-focusing due to the high-permeability
383 streaks is clearly visible.

384 Figure 5(a) shows the convergence at the final time $T = 1$ in the L^2 norm
385 for varying time-steps Δt . All schemes show convergence rates of $\mathcal{O}(\Delta t)$.
386 There is now a distinct difference between ETD1 method with Krylov or Léja
387 point technique and the implicit and semi-implicit integrators. The EDT1
388 methods displays a clear improvement in the error constant. Figure 5(b)
389 depicts the L^2 error at $T = 1$ as a function of CPU time. The ETD1 based
390 schemes are significantly more accurate and computationally more efficient
391 than (semi-)implicit schemes. They require between 10 and 100 times less
392 computational effort to achieve the same reduction in numerical error. The
393 Léja point method has also a small computational advantage over the Krylov
394 subspace technique.

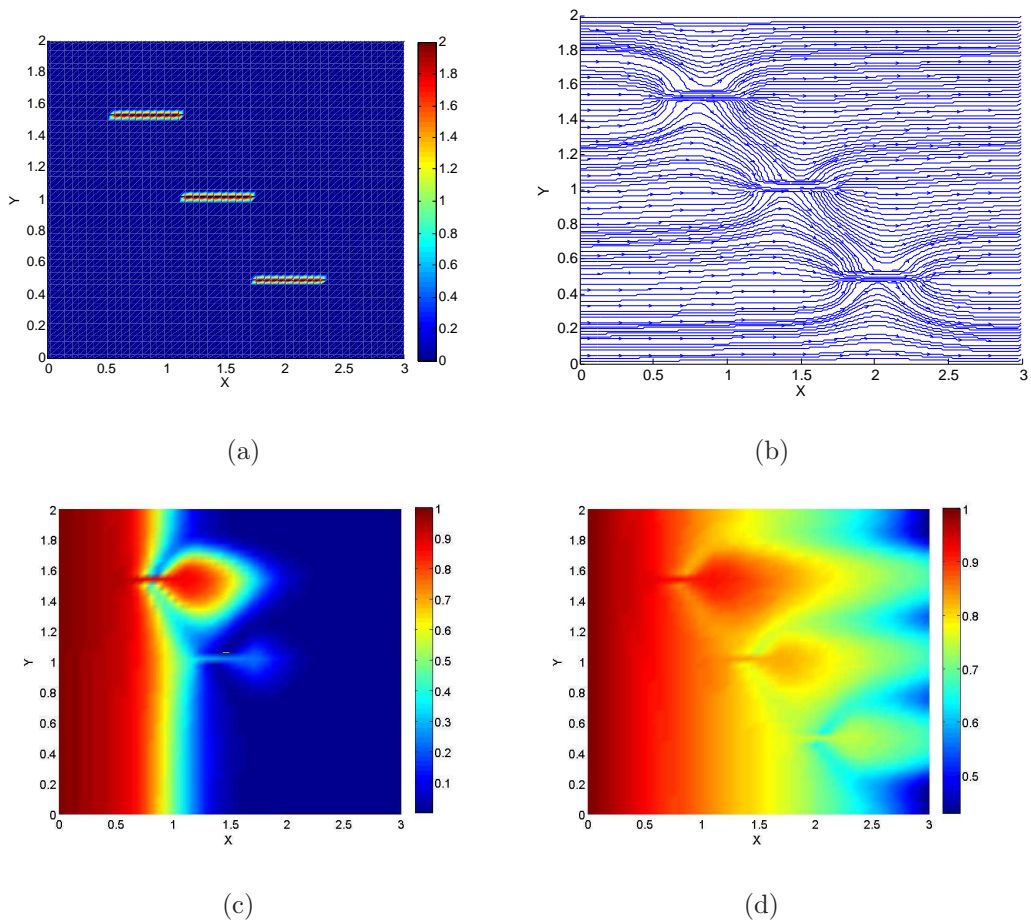


Figure 4: Numerical experiments for the non-linear ADR problem in a deterministic heterogeneous porous media (Problem 3). (a) shows the log of permeability field, (b) shows the velocity streamlines, (c) shows the concentration at $t = 0.3$ and (d) shows the concentration field at $T = 1$.

395 *4.4. Stochastic heterogeneous porous media with non-linear reaction*

396 We finally apply the ETD1 method to a stochastically generated permeability field. Stochastic permeability fields are commonly used to represent
 397 the unknown heterogeneity in the subsurface. We use the Karhunen-Loeve
 398 numerical expansion [39] to generate the random permeability field from
 399

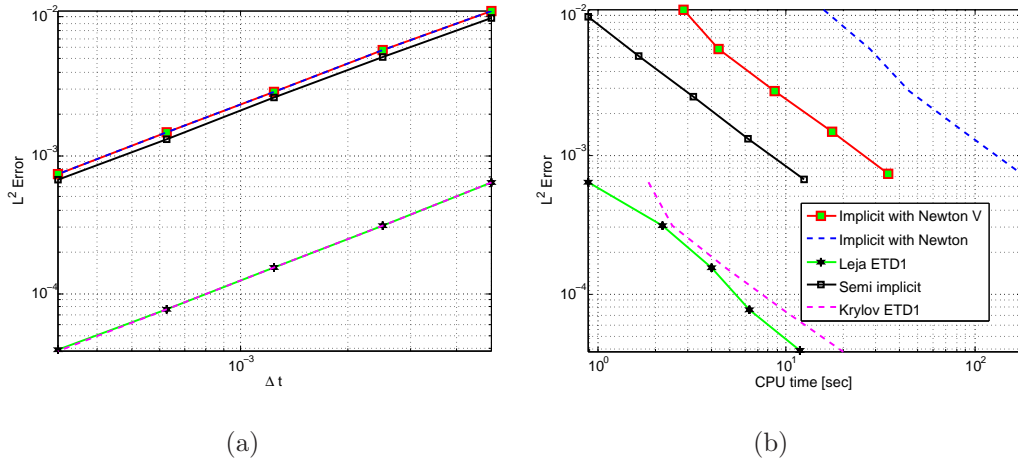


Figure 5: (a) Convergence of the L^2 norm at $T = 1$ as a function of Δt . (b) The L^2 norm at $T = 1$ as a function of CPU time. Both plots are for the non-linear ADR in a deterministic heterogeneous porous media (Problem 3). Although all time integrators display a convergence rate of $\mathcal{O}(\Delta t)$, there is clear improvement in the error constant. Hence the ETD1 schemes are significantly more efficient than (semi-)implicit methods, with the real Léja point method being most efficient.

400 a log-normal distribution with an exponentially decaying space correlation.

401 The correlation in the field is given by

$$Q((x_1, y_1); (x_2, y_2)) = \frac{1}{4b_1b_2} \exp\left(-\frac{\pi}{4} \left[\frac{(x_2 - x_1)^2}{b_1^2} + \frac{(y_2 - y_1)^2}{b_2^2} \right]\right),$$

402 where b_1 and b_2 are the spatial correlation lengths in x -direction and y -

403 direction, respectively, and given by $b_1 = 0.4$ and $b_2 = 0.2$. We used the

404 first 30 terms in the Kahunen-Loeve numerical expansion. We used the same

405 stochastically generated permeability field to evaluate all time integrators.

406 The domain is given by $\Omega = [0, 3) \times [0, 2)$ with $\Delta x = 1/10$ and $\Delta y = 1/15$.

407 The dispersion tensor has the entries $D_1 = 10^{-3}$, $D_2 = 10^{-4}$ and the viscosity

408 $\mu = 1$. The maximum local Péclet number is $Pe_{loc} = 1649.3$.

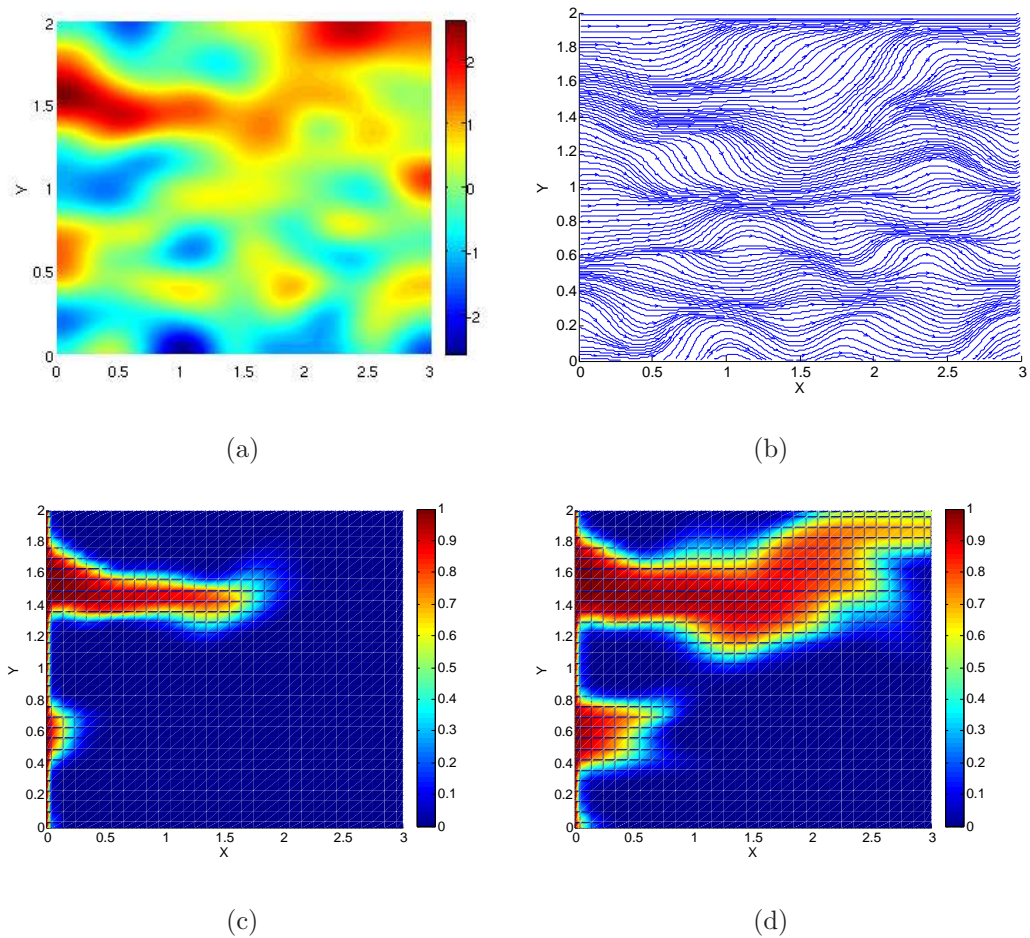


Figure 6: Numerical experiments for non-linear ADR problem in a stochastic heterogeneous porous media (a) shows the log of permeability field, (b) shows the velocity streamlines, (c) shows the concentration at $t = 0.2$ and (d) shows the concentration at $T = 1$.

409 Figure 6(a) shows the log of the permeability field, which varies over
 410 6 orders of magnitude ranging from 10^{-3} to 10^3 . Figure 6(b) shows the
 411 corresponding streamlines, which show how flow is focused into regions of
 412 high permeability. Advection rates are significantly higher in regions of high-
 413 permeability, reflected by the close streamline spacing, compared to regions

414 of low permeability. Figure 6(c) shows the concentration at $t = 0.2$ and
 415 Figure 6(d) the concentration at $T = 1$. Both show flow flow-focusing into
 416 the high-permeability regions.

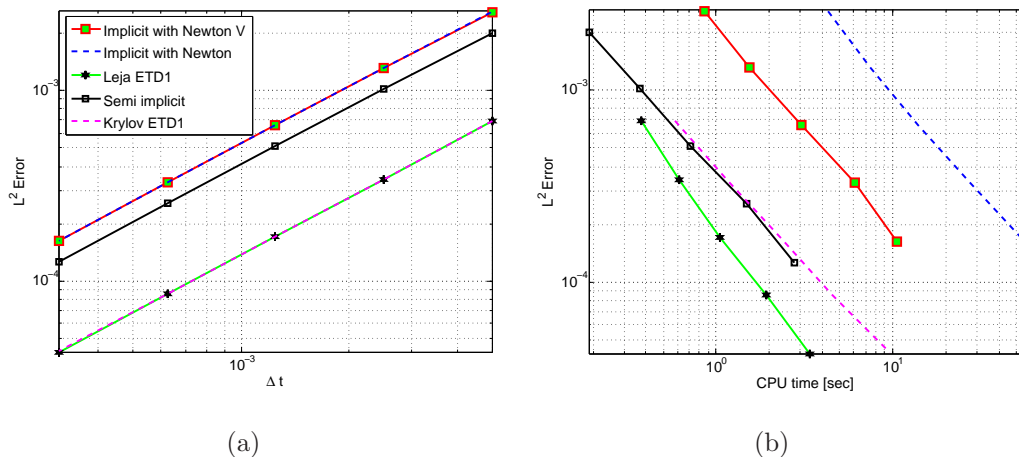


Figure 7: (a) Convergence of the L^2 norm at $T = 1$ as a function of Δt . (b) The L^2 norm at $T = 1$ as a function of CPU time. Both plots are for the non-linear ADR in a stochastically generated porous media (Problem 4).

417 Figure 7(a) shows the convergence of the L^2 norm at $T = 1$ as a function of
 418 Δt . As in all our previous applications, all schemes have similar convergence
 419 rates of $\mathcal{O}(\Delta t)$, but there is a clear improvement in the error constant for the
 420 ETD1 schemes. Figure 7(b) shows the L^2 error as a function of CPU time.
 421 The ETD1 methods clearly outperform the implicit time-integrators, with
 422 the Léja point based scheme being slightly more efficient than the Krylov
 423 subspace based methods. The latter shows a similar performance as the
 424 semi-implicit method. Table 1 compares the CPU time necessary to perform
 425 3200 steps of the ETD1 integration using the real Léja point method and the
 426 Krylov subspace technique. We analysed how many Léja points are required
 427 for the first step for different spatial discretisations ranging from 100×100

428 grid points to 500×2000 grid points. For the largest problem with 10^6
 429 unknowns only 10 Léja points are required. The total CPU time necessary
 430 to find the solution at final time $T = 1$ is 5293.3 seconds.

431 For the Krylov subspace method (with $m = 6$) the total CPU time re-
 432 quired to find the solution at the final time $T = 1$ is 14693 seconds. We
 433 observe that the real Léja point method seems more efficient than the Krylov
 434 implementation, taking approximately half the CPU time. We have tested
 435 several values for m and due to the reasons discussed previously, we do not
 436 think that the Krylov subspace technique will be more efficient than the
 437 real Léja point method for other values of m . Nevertheless, this example
 438 demonstrates that ETD1 methods are probably applicable to large-scale 3D
 439 reservoir simulations with several million unknowns.

N_x	N_y	$M_{\text{Léja}}$	CPU time [sec] Léja	CPU time [sec] Krylov ($m = 6$)
100	100	6	21	54
200	200	7	123	316
100	1000	7	430	889
200	1000	8	911	2349
100	3000	10	1589	2715
500	2000	10	5293	14693

Table 1: CPU time for the real Léja points and Krylov subspace methods used in Problem 4 as a function of various grid sizes. N_x is the number of subdivisions in the x direction and N_y the number in the y direction. Table shows the number of Léja points used for the first step $M_{\text{Léja}}$ and the CPU time to perform 3200 steps of the ETD1 method using the Léja point method and Krylov subspace technique (with $m = 6$).

440 5. Concluding remarks

441 We have developed an exponential time integrator of order one (ETD1)
442 where the matrix exponential is computed with either real fast Léja points
443 techniques or a Krylov subspace technique. We have applied it to a variety of
444 linear and non-linear advection-diffusion-reaction problems in homogeneous
445 as well as highly heterogeneous porous media where the spatial discretisa-
446 tion was achieved by standard upwind-weighted finite volume meshes on non-
447 uniform rectangular grids. The largest problems comprised 10^6 unknowns.
448 We compared the performance of the ETD1 method to standard semi-implicit
449 and implicit time integrators. Transport in our example applications was ad-
450 vection as well as diffusion dominated. All our numerical examples demon-
451 strate that the ETD1 scheme is highly competitive compared to standard
452 time integrators. This competitiveness comprises two components: efficiency
453 and accuracy. Generally, the ETD1 method requires at least 10 times less
454 computational cost compared to implicit time integrators to reduce the nu-
455 merical error to a certain value. Semi-implicit time integrators perform at
456 best similar to our ETD1 method. The real fast Léja points technique is
457 on average equivalent or more efficient than the Krylov subspace technique.
458 A similar observation was made in Martinez et al. [25] and Bergamaschi et
459 al. [26] for example applications with constant dispersion tensors, uniform
460 velocity fields, and low Péclet number flows, where the spatial discretisation
461 was achieved by finite difference and finite element space discretisation. A
462 single computation of ETD1 with real fast Léja points requires a few seconds
463 on a standard PC, even with our uncompiled Matlab code. Importantly, the
464 CPU time scales linearly with the number of unknowns, which implies that

465 ETD1 could be readily applied to large-scale 3D reservoir simulations with
466 several million of unknowns. It hence may become a viable alternative to
467 other scalable solvers such as hierarchical algebraic multigrid methods [40]
468 or multi-scale methods (e.g, [41, 42, 43]) which are commonly used for large-
469 scale simulations of flow and transport in heterogeneous porous media.

470 **6. Acknowledgements**

471 We thank three anonymous reviewers for their positive and constructive
472 comments and Prof. E. V. Vorozhtsov for editorial handling. This work
473 was supported, in part, by the initiative “Bridging the Gaps between Math-
474 ematics and Engineering” at Heriot-Watt University. S. Geiger thanks the
475 Edinburgh Collaborative of Subsurface Science and Engineering, a joint re-
476 search institute of the Edinburgh Research Partnership in Engineering and
477 Mathematics, for financial support.

478 **References**

- 479 [1] M. A. Christie and M. J. Blunt, Tenth SPE comparative solution project:
480 A comparison of upscaling techniques, *SPE Reserv. Eval. Eng.* 4(4)
481 (2001) 308–317.
- 482 [2] S. K. Matthäi and M. Belayneh, Fluid flow partitioning between frac-
483 tures and a permeable rock matrix, *Geophys. Res. Lett.* 31(7) (2004)
484 L07602 doi:10.1029/2003GL019027.
- 485 [3] B. Berkowitz, A. Cortis, M. Dentz, and H. Scher, Modeling non-Fickian
486 transport in geological formations as a continuous time random walk,
487 *Rev. Geophys.* 44(2) (2006) RG2003 doi:10.1029/2005RG000178.

- 488 [4] O. Cirpka and P. Kitanidis, Characterization of mixing and dilution
489 in heterogeneous aquifers by means of local temporal moments, *Water*
490 *Resour. Res.* 36(5) (2000) 1221–1236.
- 491 [5] A. M. Tartakovsky, G. Redden, P. L. Lichtner, T. D. Scheibe, and
492 P. Meakin, Mixing-induced precipitation: experimental study and multi-
493 scale numerical analysis, *Water Resour. Res.* 44(6) (2008) W06S04
494 doi:10.1029/2006WR005725.
- 495 [6] A. M. Tartakovsky, G. D. Tartakovsky, and T. D. Scheibe. Effects of
496 incomplete mixing on multicomponent reactive transport, *Adv. Water*
497 *Resour.* 31(11) (2009) 1674–1679 .
- 498 [7] M. Christie, V. Demyanov, and D. Ebras, Uncertainty quantification
499 for porous media flows, *J. Comput. Phys.* 217(1) (2006) 143–158.
- 500 [8] D. A. Knoll, L. Chacon, L. G. Margolin and V. A. Mousseau, On
501 balanced approximations for time integration of multiple time scale sys-
502 tems, *J. Comput. Phys.* 185(2) (2003) 583–611.
- 503 [9] D. L. Ropp, J. N. Shadid, and C. C. Ober, Studies of the accuracy of
504 time integration methods for reaction-diffusion equations, *J. Comput.*
505 *Phys.* 194(2) (2004) 544–577.
- 506 [10] G. Strang, On the construction and comparison of difference schemes,
507 *SIAM J. Numer. Anal.* 5(3) (1968) 506–517.
- 508 [11] C. I. Steefel and K. T. B. MacQuarrie, Approaches to modeling of
509 reactive transport in porous media, in: P. C. Lichtner, C. I. Steefel, and

- 510 E. H. Oelkers (Eds.), *Reviews in Mineralogy and Geochemistry Volume*
511 34, Mineralogical Society of America, Chantilly, 1996, pp. 83–129.
- 512 [12] U. M. Ascher, S. J. Ruuth, and B. T. R. Wetton, Implicit explicit
513 methods for time dependent partial differential equations, *SIAM J.*
514 *Numer. Anal.* 32(3) (1995) 797–823.
- 515 [13] M. G. Gerritsen and L. J. Durlofsky, Modeling fluid flow in oil reservoirs,
516 *Annu. Rev. Fluid Mech.* 37 (2005) 211–238.
- 517 [14] M. R. Thiele, R. P. Batycky and F. Orr, Simulating flow in heteroge-
518 neous systems using streamtubes and streamlines, *SPE Reservoir Eng.*
519 11(1) (1996) 5–12.
- 520 [15] G. DiDonato and M. J. Blunt, Streamline-based dual-porosity simula-
521 tion of reactive transport and flow in fractured reservoirs, *Water Resour.*
522 *Res.* 40(4) (2004) W04203 doi:10.1029/2003WR002772.
- 523 [16] R. D. Hornung and J. A. Trangenstein, Adaptive mesh refinement and
524 multilevel iteration for flow in porous media, *J. Comput. Phys.* 136(2)
525 (1997) 522–545.
- 526 [17] H. Karimabadi, J. Driscoll, Y. A. Omelchenko, and N. Omid, A new
527 asynchronous methodology for modeling of physical systems: breaking
528 the curse of courant condition, *J. Comput. Phys.* 205(2) (2005) 755–775.
- 529 [18] Y. A. Omelchenko and H. Karimabadi, Self-adaptive time integration
530 of flux-conservative equations with sources, *J. Comput. Phys.* 216(1)
531 (2006) 179–194.

- 532 [19] B. Minchev and W. Wright, A review of exponential integrators for
533 first order semi-linear problems, *Preprint 2/2005, Norwegian Univer-*
534 *sity of Science and Technology, Trondheim Norway 2005*, available at,
535 <http://www.math.ntnu.no/preprint/numerics/2005/N2-2005.pdf>.
- 536 [20] A. K. Kassam and L. N. Trefethen, Fourth-order time stepping for stiff
537 PDES, *SIAM J. Comput.* 26(4) (2005) 1214–1233.
- 538 [21] J. Baglama, D. Calvetti, and L. Reichel, Fast Léja points, *Electron.*
539 *Trans. Num. Anal.* 7 (1998) 124–140.
- 540 [22] L. Bergamaschi, M. Caliari, and M. Vianello, The RELPM exponential
541 integrator for FE discretizations of advection-diffusion equations, in:
542 M. Bubak, G. D. Van Albada, P. Sliot (Eds.), *Lecture Notes in Com-*
543 *puter Sciences Volume 3039*, Springer Verlag, Berlin Heidelberg, 2004,
544 pp. 434–442.
- 545 [23] M. Hochbruck and C. Lubich, On Krylov subspace approximations to
546 the matrix exponential operator, *SIAM J. Numer. Anal.* 34(5) (1997)
547 1911–1925.
- 548 [24] R. B. Sidje, Expokit: A software package for computing matrix expo-
549 nentials, *ACM Trans. Math. Software* 24(1) (1998) 130–156.
- 550 [25] A. Martinez, L. Bergamaschi, M. Caliari, and M. Vianello, A mas-
551 sively parallel exponential integrator for advection-diffusion models, *J.*
552 *Comput. Appl. Math.* 231(1) (2009) 82–91.

- 553 [26] L. Bergamaschi, M. Caliari, A. Martinez, and M. Vianello, Comparing
554 Léja and Krylov approximations of large scale matrix exponentials,
555 *Comput. Sci. – ICCS* 3994 (2006) 685–692.
- 556 [27] M. Caliari, M. Vianello, and L. Bergamaschi, Interpolating discrete
557 advection diffusion propagators at Léja sequences, *J. Comput. Appl.*
558 *Math.* 172(1) (2004) 79–99.
- 559 [28] M. Caliari, M. Vianello, and L. Bergamaschi. The LEM exponential
560 integrator for advection–diffusion–reaction equations. *J. Comput. Appl.*
561 *Math.* 210(1-2) (2007) 56–63.
- 562 [29] M. Caliari and A. Ostermann, Implementation of exponential
563 Rosenbrock-type integrators, *Appl. Numer. Math.* 59(3-4) (2009) 568–
564 581.
- 565 [30] R. Eymard, T. Gallouet, and R. Herbin, Finite volume methods, in:
566 P. G. Ciarlet, J. L. Lions (Eds.), Handbook of Numerical Analysis
567 Volume 7, North-Holland, Amsterdam, 2000, pp. 713–1020.
- 568 [31] P. Knabner and L. Angermann, Numerical methods for elliptic and
569 parabolic partial differential equations solution, Springer Verlag, Berlin,
570 2003.
- 571 [32] S. M. Cox and P. C. Matthews, Exponential time differencing for stiff
572 systems, *J. Comput. Phys.* 176(2) (2002) 430–455.
- 573 [33] H. Berland, B. Skaflestad, and W. Wright, A matlab package for ex-
574 ponential integrators, *ACM Trans. Math. Software* 33(1) (2007) Article
575 No. 4.

- 576 [34] J. W. Thomas, Numerical partial differential equations: finite difference
577 methods, Springer Verlag, Berlin Heidelberg New York, 1995.
- 578 [35] M. Caliari, Accurate evaluation of divided differences for polynomial
579 interpolation of exponential propagators, *Computing* 80(2) (2007) 189–
580 201.
- 581 [36] C. Moler and C. Van Loan, Ninteen Dubious Ways to Compute the
582 Exponential of a Matrix, Twenty–Five Years Later, *SIAM Review* 45(1)
583 (2003) 3–49.
- 584 [37] G. H. Golub and C. F. Van Loan, Matrix computations, third ed., Johns
585 Hopkins University Press, Baltimore, 1996.
- 586 [38] C. Zoppou and J. H. Knight, Analytical solution of a spatially variable
587 coefficient advection-diffusion equation in up to three dimensions, *Appl.*
588 *Math. Model.* 23(9) (1999) 667–685.
- 589 [39] R. G. Ghanem and P. D. Spanos, Stochastic finite elements, Springer
590 Verlag, New York, 2003.
- 591 [40] K. Stüben, A review of algebraic multigrid, *J. Comput. Appl. Math.*
592 128(1-2) (2001) 281–309.
- 593 [41] T. Hou and X. Wu, A multiscale finite element method for elliptic
594 problems in composite materials and porous media, *J. Comput. Phys.*
595 134(1) (1997) 169–189.
- 596 [42] Y. Efendiev, T. Hou, and X. Wu, Convergence of a nonconformal mul-

597 tiscale finite element method, *SIAM J. Numer. Anal.* 37(3) (2000) 888–
598 910.

599 [43] P. Jenny amd H. A. Tchelepi, Multi-scale finite-volume method for
600 elliptic problems in subsurface flow simulation, *J. Comput. Phys.* 187(1)
601 (2003) 47–67.